JACS
JOURNAL OF THE AMERICAN CHEMICAL SOCIETY

Article

pubs.acs.org/JACS

Single Molecule FRET Analysis of the 11 Discrete Steps of a DNA Actuator

Lasse L. Hildebrandt,[†] Søren Preus,[†] Zhao Zhang,[†,‡,§] Niels V. Voigt,[†,‡,∥] Kurt V. Gothelf,[†,‡] and Victoria Birkedal*[,†]

[†]Interdisciplinary Nanoscience center (iNANO) and Centre for DNA Nanotechnology (CDNA), Aarhus University, Gustav Wieds vej 14, 8000 Aarhus, Denmark

[‡]Department of Chemistry, Aarhus University, Langelandsgade 140, 8000 Aarhus, Denmark

Web-Enhanced Feature *Supporting Information*

ABSTRACT: DNA hybridization allows the design and assembly of dynamic DNA-based molecular devices. Such structures usually accomplish their function by the addition of fuel strands that drive the structure from one conformation to a new one or by internal changes in DNA hybridization. We report here on the performance and robustness of one of these devices by the detailed study of a dynamic DNA actuator. The DNA actuator was chosen as a model system, as it is the device with most discrete states to date. It is able to reversibly slide between 11 different states and can in principle function both autonomously and nonautonomously. The 11 states of the actuator were investigated by single molecule Förster Resonance Energy Transfer (smFRET) microscopy to obtain information on the static and dynamic heterogeneities of the device. Our results show that the DNA actuator can be effectively locked in several conformations with the help of well-designed DNA lock strands. However, the device also shows pronounced static and dynamic heterogeneities both in the unlocked and locked modes, and we suggest possible structural models. Our study allows for the direct visualization of the conformational diversity and movement of the dynamic DNA-based device and shows that complex DNA-based devices are inherently heterogeneous. Our results also demonstrate that single molecule techniques are a powerful tool for structural dynamics studies and provide a stringent test for the performance of molecular devices made out of DNA.

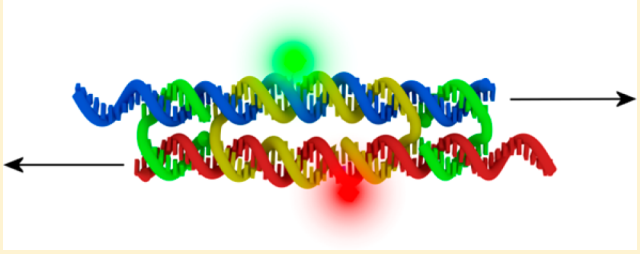

INTRODUCTION

A variety of DNA-based molecular devices can be designed using the dynamic nature of DNA hybridization.[1,2] The operation of these devices is often based on conformational changes of the DNA structure typically between two or three different states. Transition between a B and Z form of DNA structures was used to make the first dynamical device based on DNA.[3] Subsequent structures range from small DNA hairpins, which can act as molecular beacons[4] or multistate switches,[5,6] to larger 2D and 3D structures capable of changing their structure.[7−9] Small DNA mechanical devices[5] have also been used in combination with larger DNA structures for complex operation in an assembly line.[10] However, increasing the complexity of DNA-based devices also increases the chance of alternative, stable conformations that may compromise performance. It remains an open question just how complex DNA-based mechanical nanodevices can get without sacrificing reliability.

Single-molecule techniques allow the study of individual DNA devices independently, thus providing direct insight into sample static and dynamic heterogeneity.[11] In particular, single molecule Förster Resonance Energy transfer microscopy (smFRET) can provide a detailed view of structural dynamics of DNA structures.[12] The method gives an insight into the device heterogeneity during operation. smFRET has previously revealed that complex DNA structures can be very heterogeneous, such as in the case of a DNA tweezer[13] and a DNA walker.[14] On the basis of such studies, researchers have recently been able to significantly improve the operational performance of a DNA walker device.[15] Additionally, smFRET has the ability to image the fast dynamical behavior of complex devices at the single-molecule level in real time and has provided invaluable information on the dynamics of DNA hybridization[16] as well as on conformational dynamics of DNA structures, such as holiday junctions[17] and DNA G-quadruplexes.[18] Holliday junctions have also provided the basis for a dynamical DNA device showing metronome-like dynamics between two conformational states.[19] In a recent article, DNA hybridization rates were shown to critically depend on the density of the target strands.[20] However, the potential of including autonomous dynamical behavior in DNA devices and controlling the timing between different reactions is far from being fully explored in DNA nanotechnology. Direct observation of the movement of DNA devices during operation is one of the ultimate tests of their performance.

Received: March 13, 2014
Published: May 23, 2014

   dx.doi.org/10.1021/ja502580t | J. Am. Chem. Soc. 2014, 136, 8957−8962

Here, we use smFRET microscopy to obtain information about the robustness and performance of a DNA actuator device that has 11 discrete states.[21] This device is structurally very simple, however it is the device with the highest number of geometrically controlled states (Figure 1). The actuator was designed to have two pistons that can slide with respect to each other up to a total distance of ~7 nm. The sliding is made possible by the fact that the central part of the actuator, i.e., the roller strand, is complementary to a large region on both of the two piston strands. The dynamic movement of the actuator is shown in the attached animation; see Web enhanced feature. The device has the potential to move without the addition of fuel strands. Additionally, each of the 11 states of the actuator can be accessed independently by the addition of one of 11 different DNA lock strands. The lock strands are designed to hybridize to the ends of both piston arms locking the movement of the device in an addressable way. Thus, the actuator holds the capability of operating either in a semistatic way with the use of lock strands or in an intrinsically dynamic way without the lock strands. Our results show that the DNA actuator displays pronounced static and dynamic heterogeneities in all locked and unlocked states and such properties of the system are hidden in ensemble measurements.[21] We show that these heterogeneities are sensitive to small changes in the sequence of the lock strands, which demonstrates how DNA sequences can be used to fine-tune the properties of DNA-based devices. We argue that such heterogeneity is an inherent property of all DNA-based dynamic devices in which a few strands are designed to exist in multiple conformational states and this has to be taken into account when designing and optimizing the performance of DNA-based nanodevices.

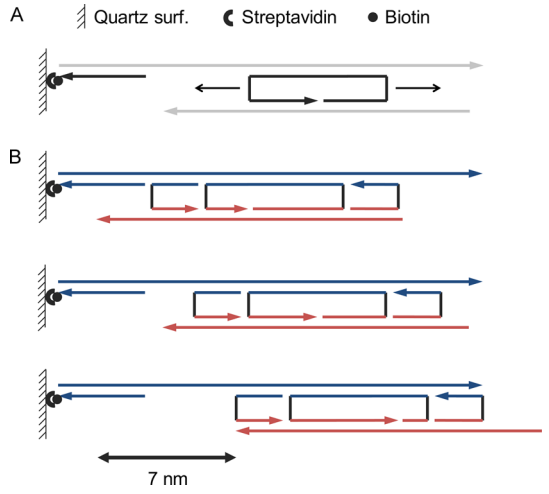

Figure 1. Schematic illustration of the surface immobilized DNA actuator. (A) Unlocked DNA actuator. The central roller is shown in black and the two piston strands are shown in gray. (B) Locked DNA actuator in state 0, 5, and 10. Piston A is shown in blue and Piston B is shown in red.

RESULTS AND DISCUSSION

By attaching a donor and acceptor fluorophore on each of the two pistons, respectively, it is possible to follow the movement of the DNA device. Using FRET spectroscopy, we have previously characterized the movement of the DNA actuator upon successive addition and removal by strand displacement of lock strands.[21] However, results obtained by ensemble FRET studies can only reflect an average conformation change on a large number of molecules. Single-molecule studies allow uncovering the true dynamic and static heterogeneities of the DNA-actuator population. These investigations were done on surface immobilized DNA actuators using an alternating laser excitation scheme (ALEX) and allow the behavior of individual molecules to be followed over time. While the DNA actuator used in the present study is modified from the original design to allow surface immobilization, the current actuator shows similar ensemble properties and behavior as previous samples (Supporting Information, (SI) Figures S2 and S3).

The DNA device was locked in each of the 11 states. FRET efficiencies extracted from the peak value of the smFRET distributions are shown in Figure 2A, and the smFRET histograms for all states of the actuator are shown in Figure 2B. The measured FRET efficiencies follow a predicted pattern going from state 0 to state 10, consistent with the fact that the

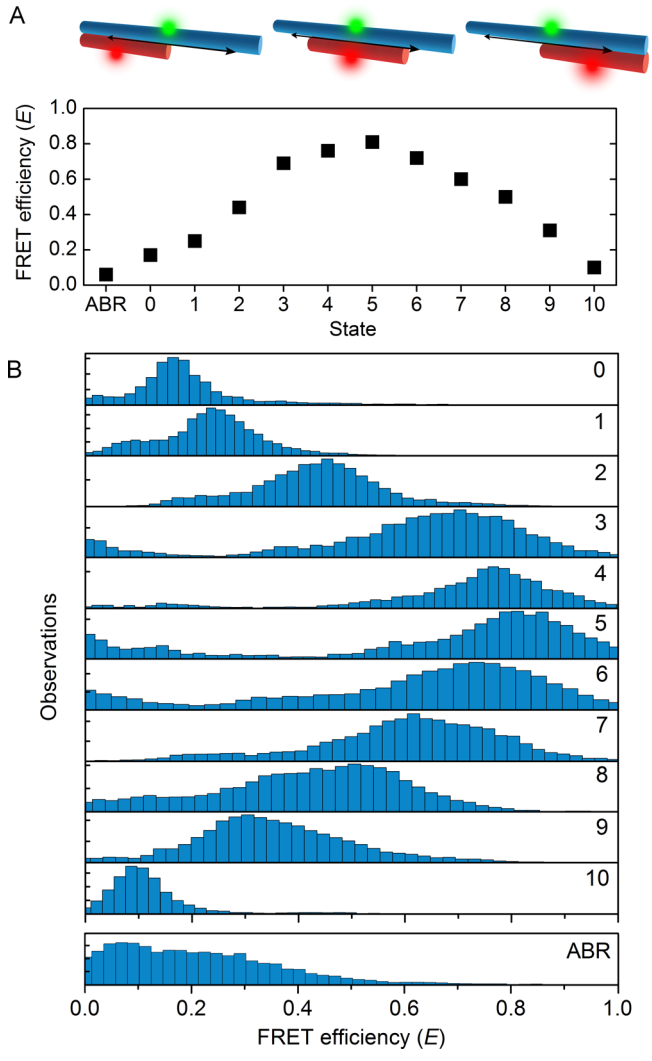

Figure 2. smFRET characterization of the DNA actuator. (A) FRET efficiency determined from the peak value of the smFRET histograms of the 11 states of the actuator. Top: Schematic illustration of the actuator in state 0, 5, and 10. Only the two piston arms are shown for simplicity. Piston A in blue and Piston B in red. (B) smFRET efficiency distribution histograms for all states of the locked actuator from 0 to 10 showing device heterogeneity. ABR denotes the unlocked actuator. The y-tick labels mark steps of 250 frames.

dx.doi.org/10.1021/ja502580t | J. Am. Chem. Soc. 2014, 136, 8957−8962

actuator pistons move with respect to each other. More specifically, the distance of the two fluorophores is largest at state 0 and state 10, while smallest at state 5, according to the design.

While the same overall trend in FRET efficiency is observed in ensemble and single-molecule experiments, the smFRET histograms show several populated states in each locked mode of the actuator (Figure 2B). Figure 3 shows the percentage of molecules that are in the desired conformation for each locked state of the DNA actuator. We assigned molecules to a given desired main state if their average FRET efficiency was within the full width half-maximum of the dominant peak in the smFRET histograms shown in Figure 2B. We excluded molecules in which a dynamic behavior was observed, as their average FRET value is not representative of a given state of the actuator. Overall, under the current experimental conditions, this method identified 50−80% of the devices to be in the desired state, depending on the sequence of the lock.

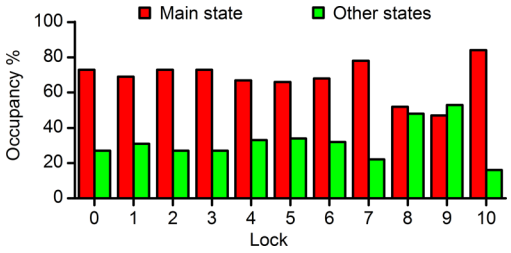

Figure 3. Relative fraction of molecules occupying the main state compared to alternative states in each locked mode of the actuator. The main state is defined as the one near the peak value of the corresponding FRET histogram in Figure 2. The histogram was obtained by counting individual molecules.

Several kinds of heterogeneity are observed in Figure 2. (1) Low FRET efficiency peaks between $E = 0$ and $E = 0.2$ are observed in FRET distribution histograms for almost all states of the actuator. Low FRET peaks are often observed in single-molecule histograms that arise from molecules where the acceptor has bleached. However, these events have been sorted out from the presented data by the use of the ALEX technique.[22] The observed low FRET peaks likely arise from contributions from molecules where the lock strands are not fully hybridized and the actuator is fully or partially unlocked (vide infra). (2) The width of the FRET efficiency distribution varies from state to state. For example, states 2 and 8 have similar mean FRET values but the FRET efficiency distribution is narrower in state 2 than in state 8. This indicates that several neighboring states of the actuator are significantly populated in the latter case. (3) The FRET distribution of the unlocked configuration is broad, as expected, but centered at low FRET efficiencies. This shows that the central roller has an unevenly distributed preference for different conformations of the actuator. In comparison, actuators in most locked configurations show narrower distributions.

Our measurement configuration additionally allows us to follow each molecule in time and thus identify both static and dynamic heterogeneities. Here, dynamic heterogeneity refers to transitions observed from one FRET efficiency state to another within the upper-limit of the observation window, which is given by the fluorophore bleaching times. Typical bleaching times are 40−400 s. The lower-limit to which dynamic transitions can be observed is given by the recording frame-rate, which is set at 200 ms in an ALEX scheme.

The individual FRET traces of the unlocked actuator show a broad range of characteristics ranging from static traces with constant FRET efficiencies (static heterogeneities, Figure 4A) to traces showing dynamics on different time scales (Figure 4, parts B and C,D, respectively). Static heterogeneities account for most of the width of the FRET efficiency distribution of the unlocked actuator observed in Figure 2B and most likely correspond to different stable conformations of the roller on the two piston arms. About 10% of the molecules showed dynamical behavior of varying characteristics (SI Figure S6).

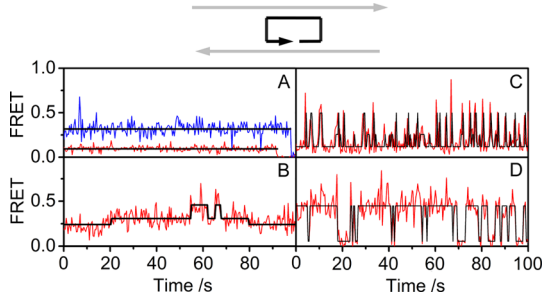

Figure 4. Examples of FRET time traces of the unlocked actuator. Top: Schematic illustration of the unlocked actuator. (A) Two static time traces with constant FRET efficiencies within the observed time-window. (B) Time trace showing dynamics in between three neighboring states. (C,D) Time traces showing fast dynamics between two or more states.

The addition of lock strands clearly guides the actuator into conformational states dictated by the sequence of the lock. In the locked configurations, the main state was always the most populated except for state 8 and 9 (Figure 3). However, as for the unlocked actuator, the individual FRET time traces of presumably locked actuators revealed different kinds of autonomous behavior of the device in each locked mode. Most time traces of locked actuators showed constant FRET efficiencies within the observed time window, however, often with varying average FRET efficiency values (Figure 5A,B). The observation of rare jumps in between two closely lying states shows that these differences in average FRET values are due to static heterogeneities of the actuator (Figure 5A). Additionally, dynamics between two or more states was observed in a subset of molecules in all locked modes (in about 10% of all

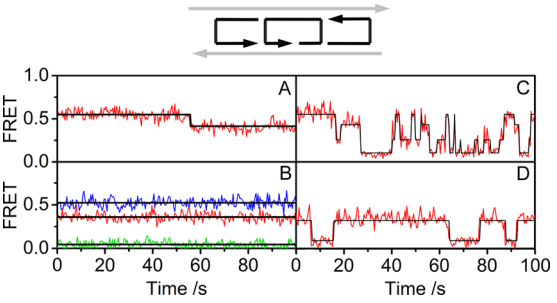

Figure 5. Examples of static and dynamic FRET time traces of the locked actuator. All traces shown were recorded using lock 8. Top: Schematic illustration of a locked actuator. (A) Transition in between main state and an alternate stable state. (B) Actuator trapped in main state (red) and two stable alternate conformations (blue and green). (C,D) Two different kinds of dynamic movement of the actuator.

dx.doi.org/10.1021/ja502580t | J. Am. Chem. Soc. 2014, 136, 8957−8962

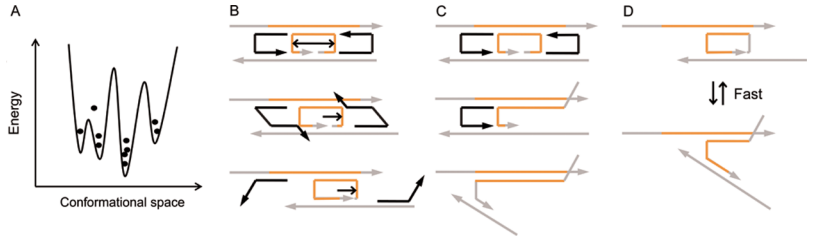

Figure 6. A tentative model for inherent heterogeneities in DNA-based mechanical devices. (A) Schematic illustration of the conformational energy landscape of a DNA-based device. Frequent transitions occur between the two left minima, while the two right minima represent trapped states. (B) Examples of the actuator getting trapped in alternative conformations due to complementarity between the roller and several positions on the two piston strands. The diagram with the corresponding sequences is shown in SI Figure S8. (C) The actuator getting trapped in alternate conformations due to full hybridization between the central roller and one of the piston arms on which it roles. (D) Proposed model that results in fast dynamics between high and low FRET states. One end of the two piston arms detaches temporarily due to a natural, thermodynamic equilibrium between the hybridized and denatured state of the 10−15 base pair overlap between the roller and the right-hand side of the lower piston.

molecules, SI Figures S6 and S7). The single-molecule data reveal frequent switching in between several conformations of the actuator both in the unlocked and the locked modes.

Conformational heterogeneity is observed both in smFRET histograms (Figure 2B) and in time traces (Figures 4 and 5). While the main state is the thermodynamically most stable conformation in almost all locked modes, as shown by Figure 3, the actuator both in unlocked and locked configurations appears to have a large number of states that are energetically close to each other and that are all populated by thermodynamic equilibria (Figure 6). This is evidenced by the observed conformational heterogeneity of the DNA actuator and the broad range of characteristics observed in the time-traces of individual molecules. The device can easily get trapped in minima which are either close (Figures 4B, 5A,B) or far (Figures 4C,D and 5D) from the intentional state, and these states are hidden in the ensemble measurements.

Examples of specific DNA conformations which may result in device heterogeneity are illustrated in Figure 6B−D. In order for the actuator to roll in between several states, the central roller must be complementary to a large region on the piston arms (some of the regions are shown in orange in Figure 6). This complementarity in between several regions inevitably results in multiple stable secondary conformations of the device, even after the addition of lock strands. For example, in all cases, conformations neighboring the main state of the locked actuator are semistable themselves (in Figure 6B and SI Figure S8). In these states, the lock strands are only partially hybridized. Additionally, the central roller may hybridize with the upper piston arm, forming an undesired duplex of up to 44 base-pairs in length while still binding to an acceptor strand through its 10−15 base overhang (Figure 6C). This structure is suggested to be the origin of the low FRET states of $E = 0-0.2$ in almost all configurations, including the unlocked actuator. The conformations illustrated in Figure 6B, in which the device is trapped in neighboring states close in energy, are consistent with the mostly static heterogeneities observed in all configurations and illustrated in Figure 5A,B. This model additionally explains why actuators in locked configurations 8 and 9 are particularly heterogeneous compared to the other states. The lock strands are 22 bases long and hybridize with 11 bases on each piston of the DNA actuator. The sequences of locks 8 and 9 differ only at two base positions and, equally important, the central G base of these two locks can hybridize on both arms of the piston (SI Figure S8). DNA hybridization can thus occur at more places with just a small energetic penalty, and the device may be able to move between close states. The very fast dynamics in between two states of low and medium FRET efficiencies observed in both the locked and unlocked modes of the actuator (Figures 4C,D and 5C) may be explained by the model shown in Figure 6D. Here one end of the two pistons of the actuator is temporarily detached due to the relatively short overlap between the roller and the lower piston in this particular region (10−15 base pairs). In this model, the observed FRET transitions are caused by a traditional dynamic equilibrium in between the hybridized and denatured state of the right part of the lower piston on the roller. The time-scales of this dynamic equilibrium are dictated by the DNA sequences of the individual strands, demonstrating how sequence design might be used to tune short-scale dynamics in DNA nanostructures.

Importantly, DNA-based devices designed to exist in several conformational states through hybridization engineering will generally possess an inherent heterogeneity. This fact may decrease the device reliability as the desired state will not be 100% populated. While the free energy of any intended conformational state can in principle be further decreased by design optimization, e.g., using longer complementary strands, the existence of semistable, secondary conformations in which the device can get trapped will always be present in multistate devices, which are based on the hybridization in between a few DNA strands. These heterogeneities are not evident from ensemble measurements, but can only be truly quantified by single-molecule techniques.

While the DNA actuator shows pronounced heterogeneities in all states, it is nevertheless interesting to see how the presence of locks allows the desired state to be mostly populated. The maximum observed yield of around 80% of the actuator in a locked configuration is at the high end compared to those of other complex DNA devices.[13,14] Autonomous and dynamic oscillation between different states can occur when the energy barrier is small. Dynamic movement between a few states was observed on different time scales in the actuator. Dynamic properties depend on the energy landscape of the different conformations and may be tuned by sequence and external conditions.

■ CONCLUSIONS

Our results allow detailed insight into the performance of a mechanical DNA actuator that serves as a model system for exploring the strengths and limitations of DNA-based mechanical devices. We find that the device can be prepared in each of the 11 states in a semi static way with about 50−80% yield. Due to the limited alphabet in DNA and the intrinsic

dx.doi.org/10.1021/ja502580t | J. Am. Chem. Soc. 2014, 136, 8957−8962

heterogeneity of DNA-based devices, it may be difficult to achieve 100% yield for a nanostructure with a large number of states. This study thus pinpoints the limitations of using DNA as a material for mechanical devices at the nanoscale. More efficient device preparation may require other routes such as scavenging of unwanted devices. However, the intrinsic heterogeneity of DNA devices led to the observation of autonomous dynamic behavior in the locked actuator. This fact can be further exploited to design devices that oscillate autonomously between different states with a controlled average frequency. Finally, single molecule studies offer a stringent test for the performance of heterogeneous molecular machines and a unique insight into how to improve their design.

METHODS AND MATERIALS

DNA Actuator Assembly. The core DNA actuator construct is composed of three single stranded DNAs (ssDNA), namely Piston A, Piston B, and a nicked circular strand connecting the two pistons R, see Figure 1. Additionally, the biotin-labeled ssDNA C is added for surface immobilization purposes. Piston strands A and B are internally labeled through a C6 type linker with Alexa555 and Alexa647 fluorophores, respectively. The device can slide into 11 different states with hybridization with lock strands. Detailed sequences can be found in the SI.

Assembly of the core DNA actuator was done by annealing equal stoichiometric quantities of the four ssDNA oligonucleotides A, B, C, and R in TAE/Mg^{2+} buffer composed of tris(hydroxymethyl)-aminomethane (Tris) base (40 mM, pH 8.0), acetic acid (20 mM), ethylenediaminetetraacetate (EDTA; 2 mM), and $MgCl_2$ (12.5 mM). Assembly efficiency was high as shown in the gel shift assay in SI Figure S1.

sm FRET Experiments and Data Analysis. DNA actuator molecules were immobilized via biotin−streptavidin linkage on a quartz coverglass for prism total internal reflection fluorescence microscopy. Fluorescence was measured using an inverted wide-field optical microscope and alternate laser excitation at 514 and 630 nm of the donor and acceptor fluorophore, respectively. Fluorescence movies of several minutes were recorded with an EMCCD camera (Andor, iXon3 897) with a 200 ms integration time per image. Typical excitation intensities were ∼0.34 and 0.09 kW/cm^2 for the green and red laser, respectively.

Sample chambers for smFRET measurements were coated with BSA-biotin and streptavidin and incubated with DNA actuator samples at a concentration of ∼30 pM for 15 min. The flow-cell was then washed with TAE/Mg^{2+} buffer, which was then replaced by the imaging buffer, consisting of TAE/Mg2+ buffer containing an oxygen scavenger system (2 mM Trolox (Sigma-Aldrich), glucose oxidase (Sigma-Aldrich, 16,67 units/ml), catalase (Sigma-Aldrich, 260 units/ml), and β-D-(+)glucose (Sigma-Aldrich, 4.5 mg/mL)). Measurements were done under flow with 2,5 mL/hour flow rate. Detailed protocols for these measurements can be found in ref 23.

To study the behavior of locked devices, samples were prepared where the DNA actuator is locked in each of the 11 states. The core DNA actuator device at a concentration of 1 nM was incubated with at least 20-fold excess of lock strands at room temperature for 30 min.

Data analysis was performed by a homemade smFRET microscopy software package iSMS.[24] Co-localized donor/acceptor fluorescence spots were identified by a combination of a fast peak search algorithm and image registration between the green and red emission channels. The resulting fluorescence time traces were analyzed, and traces showing stepwise bleaching or closely separated peaks (<7−8 pixels) were excluded from the analysis. Relative FRET efficiencies were obtained from the donor and acceptor fluorescence intensities after background and filter corrections as follows:

$$E = \frac{F_{\mathrm{FRET}}}{F_{\mathrm{FRET}} + \gamma \cdot F_{\mathrm{D}}^{\mathrm{D}}}$$

Here $F_{\mathrm{D}}^{\mathrm{D}}$ and F_{FRET} denote fluorescence intensities observed in the donor and acceptor emission channel, respectively, after donor excitation. The latter is corrected for direct excitation of the acceptor at the donor excitation wavelength and leakage of donor emission into the red emission channel using the correction factors $A_{\mathrm{direct}} = 0.10$ and $D_{\mathrm{leakage}} = 0.13$ (SI). The factor γ corrects for differences in brightness and detection efficiency between the donor and acceptor fluorophores. smFRET histograms contain only data from dual labeled molecules before fluorophore bleaching. Only the first 100 frames of each smFRET time trace were used to make these plots, so as to minimize the contribution of molecules with long time traces to the overall histogram. Each frame is an observable and the bin size is 0.02. Typical numbers of molecules collected for each locked state and for the unlocked state of the DNA actuator are ∼50−100 molecules. The γ factor value was determined to be $\gamma = 2.6$ (SI). FRET time series showing transitional dynamics were analyzed using hidden Markov modeling with the variational Bayesian expectation maximization (VBEM) technique (originally developed for vbFRET).[25] Transitional dynamics were identified, and distinguished from noise, by the anticorrelation between donor and acceptor intensities (SI Figure S4).

ASSOCIATED CONTENT

Supporting Information

Additional experimental methods, DNA sequences, and Figures S1−S8. This material is available free of charge via the Internet at http://pubs.acs.org.

Web-Enhanced Feature

A movie showing the DNA actuator movement is available in the HTML version of the paper.

AUTHOR INFORMATION

Corresponding Author

vicb@inano.au.dk.

Present Addresses

[§]Nanobiology Institute, Yale University, West Haven, CT 06516, U.S.A.

[‖]Danish Technological Institute, Kongsvang Allé 29, Aarhus C, Denmark.

Notes

The authors declare no competing financial interest.

ACKNOWLEDGMENTS

We would like to thank Asger Christian Krüger at iNANO, Aarhus University for practical assistance in the early stages of the project. This work was supported by the Danish Council for Independent Research's research carrier program Sapere Aude, the Lundbeck Foundation, and the Danish National Research Foundation grant no. DNRF81.

REFERENCES

(1) Krishnan, Y.; Simmel, F. C. *Angew. Chem., Int. Ed.* **2011**, *50*, 3124.

(2) Bath, J.; Turberfield, A. J. *Nat. Nanotechnol.* **2007**, *2*, 275.

(3) Mao, C. D.; Sun, W. Q.; Shen, Z. Y.; Seeman, N. C. *Nature* **1999**, *397*, 144.

(4) Tyagi, S.; Kramer, F. R. *Nat. Biotechnol.* **1996**, *14*, 303.

(5) Yan, H.; Zhang, X. P.; Shen, Z. Y.; Seeman, N. C. *Nature* **2002**, *415*, 62.

(6) Burns, J. R.; Preus, S.; Singleton, D. G.; Stulz, E. *Chem. Commun.* **2012**, *48*, 11088.

(7) Andersen, E. S.; Dong, M.; Nielsen, M. M.; Jahn, K.; Subramani, R.; Mamdouh, W.; Golas, M. M.; Sander, B.; Stark, H.; Oliveira, C. L.; Pedersen, J. S.; Birkedal, V.; Besenbacher, F.; Gothelf, K. V.; Kjems, J. *Nature* **2009**, *459*, 73.

(8) Aldaye, F. A.; Sleiman, H. F. *J. Am. Chem. Soc.* **2007**, *129*, 13376.

(9) Goodman, R. P.; Heilemann, M.; Doose, S.; Erben, C. M.; Kapanidis, A. N.; Turberfield, A. J. *Nat. Nanotechnol.* **2008**, *3*, 93.
(10) Gu, H. Z.; Chao, J.; Xiao, S. J.; Seeman, N. C. *Nature* **2010**, *465*, 202.
(11) Birkedal, V.; Dong, M. D.; Golas, M. M.; Sander, B.; Andersen, E. S.; Gothelf, K. V.; Besenbacher, F.; Kjems, J. *Microsc. Res. Technol.* **2011**, *74*, 688.
(12) Roy, R.; Hohng, S.; Ha, T. *Nat. Methods* **2008**, *5*, 507.
(13) Muller, B. K.; Reuter, A.; Simmel, F. C.; Lamb, D. C. *Nano Lett.* **2006**, *6*, 2814.
(14) Masoud, R.; Tsukanov, R.; Tomov, T. E.; Plavner, N.; Liber, M.; Nir, E. *ACS Nano* **2012**, *6*, 6272.
(15) Tomov, T. E.; Tsukanov, R.; Liber, M.; Masoud, R.; Plavner, N.; Nir, E. *J. Am. Chem. Soc.* **2013**, *135*, 11935.
(16) Cisse, I. I.; Kim, H.; Ha, T. *Nat. Struct. Mol. Biol.* **2012**, *19*, 623.
(17) Joo, C.; McKinney, S. A.; Lilley, D. M. J.; Ha, T. *J. Mol. Biol.* **2004**, *341*, 739.
(18) Lee, J. Y.; Okumus, B.; Kim, D. S.; Ha, T. J. *Proc. Natl. Acad. Sci. U. S. A.* **2005**, *102*, 18938.
(19) Buranachai, C.; McKinney, S. A.; Ha, T. *Nano Lett.* **2006**, *6*, 496.
(20) Johnson-Buck, A.; Nangreave, J.; Jiang, S.; Yan, H.; Walter, N. G. *Nano Lett.* **2013**, *13*, 2754.
(21) Zhang, Z.; Olsen, E. M.; Kryger, M.; Voigt, N. V.; Torring, T.; Gultekin, E.; Nielsen, M.; MohammadZadegan, R.; Andersen, E. S.; Nielsen, M. M.; Kjems, J.; Birkedal, V.; Gothelf, K. V. *Angew. Chem., Int. Ed.* **2011**, *50*, 3983.
(22) Kapanidis, A. N.; Lee, N. K.; Laurence, T. A.; Doose, S.; Margeat, E.; Weiss, S. *Proc. Natl. Acad. Sci. U. S. A.* **2004**, *101*, 8936.
(23) Kruger, A. C.; Hildebrandt, L. L.; Kragh, S. L.; Birkedal, V. In *Laboratory Methods in Cell Biology: Imaging*; Conn, P. M., Ed.; Elsevier Academic Press Inc: San Diego, 2012; Vol. *113*, p 1.
(24) Preus, S.; Birkedal, V. Manuscript in preparation.
(25) Bronson, J. E.; Fei, J. Y.; Hofman, J. M.; Gonzalez, R. L.; Wiggins, C. H. *Biophys. J.* **2009**, *97*, 3196.